Journal of Magnetic Resonance **137,** 379–388 (1999)
Article ID jmre.1998.1697, available online at http://www.idealibrary.com on IDEAL®

High-Speed Data Acquisition System and Receiver Configurations for Time-Domain Radiofrequency Electron Paramagnetic Resonance Spectroscopy and Imaging

S. Subramanian, R. Murugesan, N. Devasahayam, J. A. Cook, M. Afeworki, T. Pohida,*
R. G. Tschudin, J. B. Mitchell, and M. C. Krishna

*Radiation Biology Branch, Division of Clinical Sciences, National Cancer Institute, National Institutes of Health, Bethesda, Maryland 20892; and *Signal Processing and Control Systems Group, Computational Bioscience & Engineering Laboratory, National Cancer Institute, National Institutes of Health, Bethesda, Maryland 20892*

Received August 26, 1998; revised December 22, 1998

Design strategies, system configuration, and operation of a dual-channel data acquisition system for a radiofrequency (RF) time-domain electron paramagnetic resonance (EPR) spectrometer/imager operating at 300 MHz are described. This system was configured to incorporate high-speed analog-to-digital conversion (ADC) and summation capabilities with both internal and external triggering via GPIB interface. The sampling rate of the ADC is programmable up to a maximum of 1 GS/s when operating in a dual-channel mode or 2 GS/s when the EPR data are collected in a single-channel mode. By using high-speed flash ADCs, a pipelined 8-bit adder, and a 24-bit accumulator, a repetition rate of 230 kHz is realized to sum FIDs of 4096 points. The record length is programmable up to a maximum of 8K points and a large number of FIDs (2^{24}) can be summed without overflow before the data can be transferred to a host computer via GPIB interface for further processing. The data acquisition system can operate in a two-channel (quadrature) receiver mode for the conventional mixing to baseband. For detection using the single-channel mode, the resonance signals around the center frequency of 300 MHz were mixed with a synchronized local oscillator of appropriate frequency leading to an intermediate frequency (IF) which is sampled at a rate of 2 GS/s. Comparison of quadrature-mode and an IF-mode operation for EPR detection is presented by studying the FID signal intensity across a bandwidth of 10 MHz and as a function of transmit RF power. Imaging of large-sized phantoms accommodated in appropriately sized resonators indicates that IF-mode operation can be used to obtain distortion-free images in resonators of size 50 mm diameter and 50 mm length.

INTRODUCTION

Functional or physiological imaging techniques in biomedical research are receiving increased attention (*1, 2*). Such techniques, coupled with anatomical imaging techniques, strengthen diagnostic radiology used to detect disease states and characterize them physiologically on the basis of tissue redox status or oxygenation level, and thus guide effective therapies. Noninvasive radiologic techniques such as MRI (*1*) (blood oxygen level dependent, BOLD), PET (*3*), and ^{31}P MRS (*4*) are some of the noninvasive techniques being evaluated toward these goals. Electron paramagnetic resonance (EPR) spectroscopy is emerging as an important tool as well for obtaining physiological information in *in vivo* studies (*5–7*). Because of the relatively large linewidths of most spin probes used in EPR, continuous wave (CW) methods were preferred for data acquisition in the frequency domain to utilize the inherent advantages with phase-sensitive detection in the receiver circuits (*8–13*). Such spectroscopic studies have provided valuable information on the pO_2 levels in tumors, particularly during treatment (*6*). Imaging studies have also provided information in cardiac tissue and tumors (*14, 15*). However, because of the relatively longer times taken for spectral acquisition, imaging times were long (minutes to hours), requiring continuous infusion of the spin probe as well as appropriate gating techniques (*16*) to minimize artifacts associated with object motion during imaging experiments.

With the recent availability of single-line paramagnetic spin probes which are nontoxic, biologically compatible (*17, 18*), and water soluble and which can be intravenously or intramuscularly injected into animals, time-domain EPR imaging has become a potentially useful technique for obtaining information such as tissue redox status as well as oxygenation level. Radiofrequency (RF) EPR imaging systems operating in the time domain have been reported by us and others recently (*19–22*), employing narrow excitation pulses (50 ns) and capturing the transient responses or the free induction decay (FID) signals which are typically in the range 1–3 μs. In addition to minimal artifacts associated with object motion, advantages of time-domain EPR include potentially short imaging times as well. However, some of the considerations are: (a) minimization of the spectrometer dead time (the time gap between the trailing end of the pulse and decay of the resonator ring-down); (b) development of efficient signal acquisition and averaging capabilities to offset the loss in sensitivity inherent in EPR

1090-7807/99 $30.00

spectroscopy and imaging in the radiofrequency regime; and (c) availability of spin probes with long phase memory.

Since, at RF, the dead times can be longer than at X-band frequency, a significant portion of the exponentially decaying FID will be within the resonator ring-down time, and hence cannot be recovered. After the resonator recovers, the remaining portion of the rapidly decaying FID must be digitized at the maximum possible rate and their summation should be also at the maximum possible rate. With such capabilities, the short relaxation times of paramagnetic species can be exploited to enhance the SNR (signal-to-noise ratio) by rapid digitization and summation of the time-domain responses. This requires optimal digitization and rapid summing capabilities (*23*). Though high-speed digitizers with sampling rates greater than 1 GHz are available, the summing rates are not adequate for time-domain EPR experiments for the enhancement of the SNR. In continuation of our efforts to develop data acquisition systems (DAS) for pulsed EPR experiments (*24*, *25*), we report here a dual-channel DAS with high digitization/summation speed, operating in both the conventional baseband mode and a novel "intermediate frequency (IF)-mode" by mixing the FID signal with a frequency different from that of the transmitter.

The two-channel data acquisition system can be used in a quadrature configuration in the conventional baseband mode, which offers several distinct advantages over single-channel detection, such as: (1) enhancement in sensitivity by a factor of $\sqrt{2}$; (2) elimination of aliasing artifacts; and (3) optimal utilization of transmit RF power. For quadrature detection, the spectrometer needs to be complemented with various pulse cycling sequences (CYCLOPS) (*26*) to minimize the phase errors arising from the mismatch in the phase and gain stability of the two channels (*27*). Additional hardware, such as a second digitizer and phase shifter, will be required to implement this scheme. An alternate to the quadrature configuration in the detection scheme is evaluated by mixing the FID signal with a synchronized local oscillator frequency different from the transmitter frequency to get an intermediate frequency appropriate for the FID signal bandwidth in the specific experiment. The advantages of this system are: (1) elimination of CYCLOPS sequences, thereby minimizing the hardware complexity, and (2) flexibility of IF and bandwidth based on the imaging experiment. In this paper, we evaluate the relative efficiencies of the quadrature detection and the IF mixing schemes in the pulsed RF EPR imaging experiment.

SPECTROMETER DESIGN

The time-domain RF EPR spectrometer/imager and the subassemblies used in this study have been reported recently (*25*). Figure 1 gives the block diagram of the time-domain EPR spectrometer/imager operating at 300 MHz. The upper part of the figure shows the transmit arm, providing the gating and mixing sequences. The lower part shows the receiver arm. The SW-1 switch is utilized depending on the receiver configuration of IF or quadrature. In the single-channel mode, for mixing the induction signal to get an IF of 50 MHz, GATE-1 is open only for the duration of the transmitting pulse, which is typically from 50 to 300 ns. In the quadrature mode, Gate-1 is kept open for the entire duration of the transmit and receive times. The digitizer inputs *I* and *Q* are also changed accordingly. Figure 2 gives the timing sequence for the IF and quadrature operation. For quadrature detection, the induction signals were mixed with a carrier frequency of 300 MHz whereas in IF detection, the induction signals from the resonator were mixed with a frequency of 350 MHz. The carrier (300 MHz) and the local oscillator (350 MHz) were derived from a single-source 800-MHz frequency from an HP8340 signal generator to maintain a constant phase difference between the two for each repetition. In such a configuration, a range of offset frequencies are provided at ± 50 MHz from the resonator so as to maintain the IF in the range 0–100 MHz. Since negative frequencies need not be addressed, dual-channel detection is not required. To avoid breakthrough of the carrier frequency arising from the electromagnetic inductive effect and feedthrough (*23*), gating sequences are used as shown in Fig. 2. By suitably gating the various sources that lead to the final frequencies of 300 and 350 MHz, it can be ascertained that during the acquisition time there was no 300 MHz persisting in the receiver circuit. This prevents the resonator from receiving the carrier frequency (300 MHz) via the antennae effect, thereby preventing any unwanted artifacts in the middle of the spectrum. Further, the phase of the transmit frequency is alternated 0°/180° during the data acquisition and the corresponding FID signals are added/subtracted to the memory alternatively to eliminate any spurious signal.

Averager. A block diagram of the data acquisition system used in this study is shown in Fig. 3. The system is based on a modular design comprising of three subunits, namely: (i) sampler, (ii) summer, and (iii) processor.

The sampler contains four high-precision ADCs (TKAD10C) with a sampling rate of 500 Ms/s and a vertical resolution of 8 bits. Since interleaving techniques are used to increase the sampling rate above the maximum sampling rate of the individual ADCs, a very close matching of the ADCs in terms of gain, offset, and sampling times over the entire operating ranges is provided by control signals. A maximum interleaved sampling rate of 1 GS/s in two-channel mode or 2 GS/s in single-channel mode can be realized. Signals *I* and *Q* represent the two inputs to the digitizer. The preamplifiers provide a gain and offset for the input FID signals. Internal calibrations are also provided in the preamplifiers. Further, the preamplifiers are optimized to provide superior bandwidth (1.3 GHz), phase linearity ($\pm 2°$), and spurious free range (50 dB). However, the input range of the preamplifier is fixed at 500 mV.

All the control and timing signals are derived from the same time base. FIDs are sampled on each edge of the divided master clock for interleave mode. For the two-way interleave,

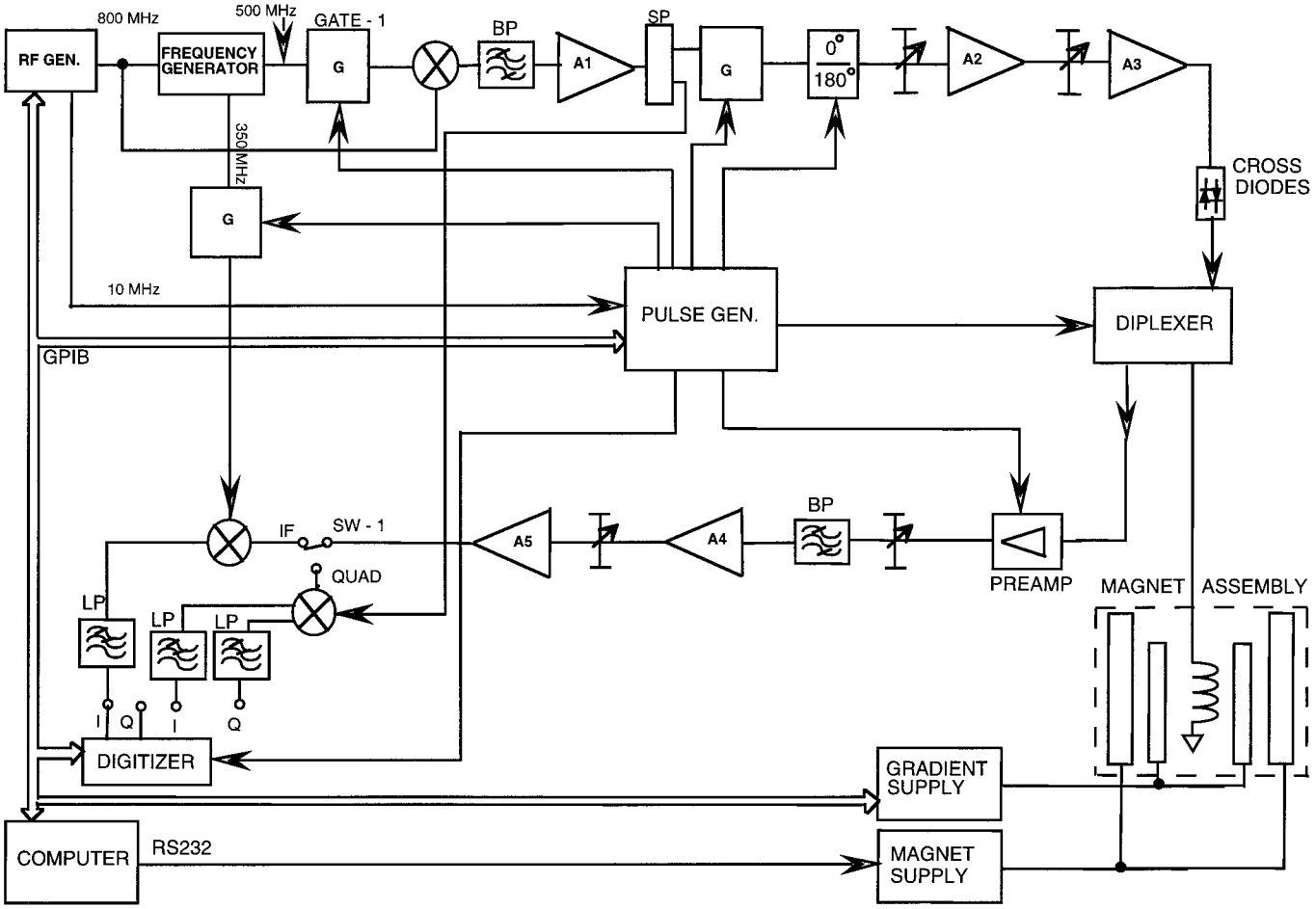

FIG. 1. Schematic of the radiofrequency EPR spectrometer operating in the conventional mode and the IF mode. The upper part of the schematic shows the generation of carrier and local oscillator frequencies from a single source of phase-locked 800 MHz derived from a Hewlett–Packard frequency synthesizer (HP 8644, Hewlett–Packard, Palo Alto, CA). In the lower part alternate methods involving single-channel IF detection and the conventional dual-channel quadrature detection are shown. Pulses and timing sequences are generated using three daisy-chained delay generators (DG 535, Stanford Research Systems, Sunnyvale, CA). Fast acquisition of data and summing were done using a custom-built Analytek 20000RV2 digitizer/summer (Tektronix, Sunnyvale, CA).

channels A and B sample on the positive edge whereas C and D sample on the negative edge. In the four-way mode, A and B sample on alternate positive edges and C and D on alternate negative edges. A trigger controller provides triggering capability from the external source and the triggering circuitry is enabled by a control signal from the pulse generator of the EPR spectrometer.

A block diagram of the summer is given in Fig. 4a. For each FID signal, two channels are provided; there are four channels in total and these four data streams are 16 bits wide. ECL logic (Motorola 100K ECLPS series) is used to implement the data channels. The input FIFO memories (IDT 72221) buffer the FID data from the sampler. The data from the input FIFOs are summed with a pipelined 8-bit adder and a 24-bit accumulator. Therefore, the summation FIFOs can accommodate 32-bit data for each of the FID signals. A detailed description of one of the channels is given in Fig.4b.

The summing process begins when the processor activates a control signal to the summer, which in turn activates the sampler to send the digitized data over the four channels. After the digitized waveforms are summed, the summer reactivates the sampler to initiate the next digitizing cycle. This process repeats until a programmed number of FIDs are summed. This programmable number is a 24-bit word and hence more than 16 million repetitions with almost real-time averaging can be completed without transferring the data to the host computer. The summation process operates simultaneously with the digitization process by the sampler when it operates in a pretrigger mode. The summing process begins when the first words have been loaded into all of the input FIFO memories. Thus, the summing process effectively overlaps the digitization process since it does not have to wait until the loading of the input FIFOs is completed. FIDs with a record length of 2K points for both the I and Q signals can be summed at a rate of 230 kHz (retrigger period of approximately 4.3 μs). The data output from the summer is 32 bits wide and provides a very high

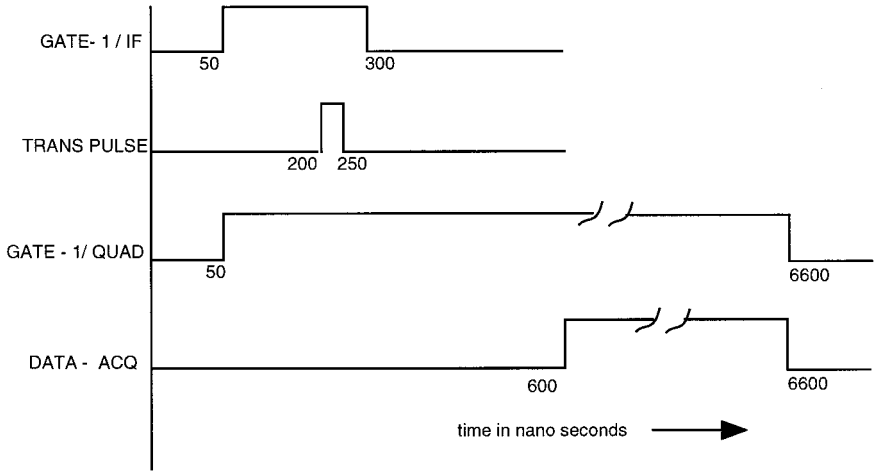

FIG. 2. Timing sequence for data acquisition in the two modes, namely conventional quadrature and the current IF modes. In the IF mode, the local oscillator which produces the 300 MHz by mixing schemes is timed out during acquisition to avoid large feedthrough at the middle of the spectrum. A dead time of approximately 300–400 ns was noticed with our low-*Q* parallel coil resonators.

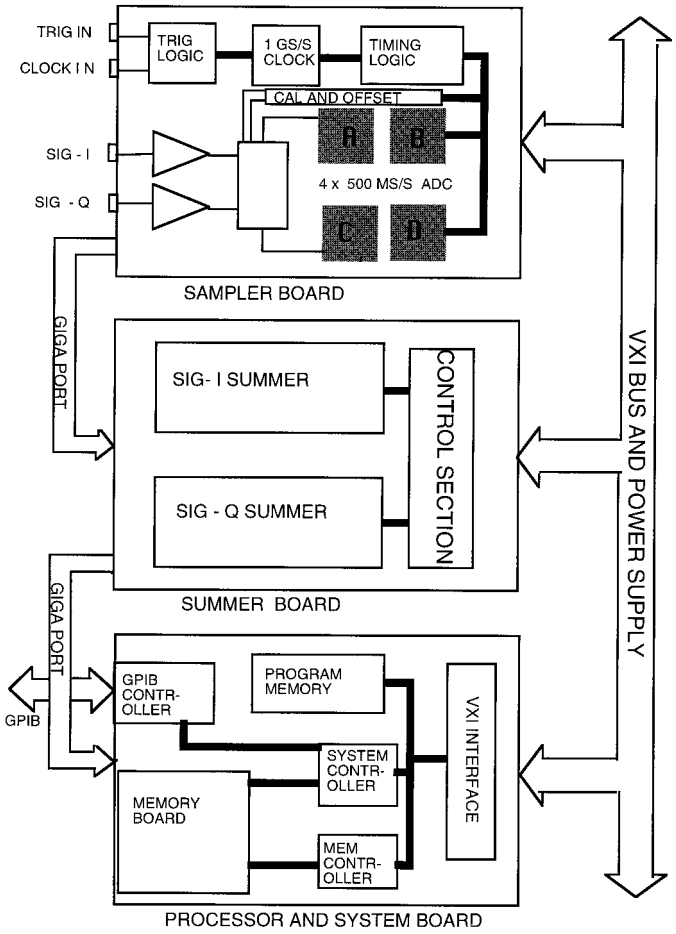

FIG. 3. Block diagram of the Analytek data acquisition system showing the submodules consisting of the sampler board, the summer board, and the processor board.

dynamic range for averaging. The summed 32-bit data is transferred in sequence to the processor as two 16-bit words.

The processor module contains a 32-bit microprocessor (Motorola 68340) with a memory of 64 MB. It supports a direct memory access (DMA) transfer at speeds of up to 1 MB/s. The National Instruments NAT4882BPL IEEE-488.2 controller is interfaced to the microprocessor. The host computer initiates the experiment through the GPIB interface. At the start of the experiment commands are sent to calibrate the hardware. After calibration, the desired data acquisition parameters such as the number of repetitions of FID, the record length, and the sampling frequency are set by the host computer using C language. After a predefined number of FIDs are summed, the data are transferred to the host computer where signal processing routines such as digital filtering, baseline correction, Fourier transform, back-projection, and image processing are carried out.

Resonator. An overcoupled parallel coil resonator (*28*) with a diameter of 25 mm and a height of 50 mm was used for detection. These dimensions were adequate for accommodating an experimental animal, such as a mouse, for imaging studies. Resonators of 50 mm diameter and 50 mm height as well as 80 mm diameter and 50 mm height were also optimized for imaging experiments. The loaded *Q* of the coil was maintained at 25. A dead time in the range of 350–500 ns was observed for these resonators for an input power of 80 W.

Spin probe. Since the time-domain responses of the spin probes should last longer than the spectrometer dead time, the charge-transfer complex *N*-methylpyridinium tetracyanoquinodimethane (NMP-TCNQ) was used. This solid charge-transfer complex spin probe has a linewidth of approximately 200 mG. This corresponds to a frequency width of 0.56 MHz and a T_2^* of 568 ns and the FID persists only for approximately 2.8 μs ($5 \times T_2^*$).

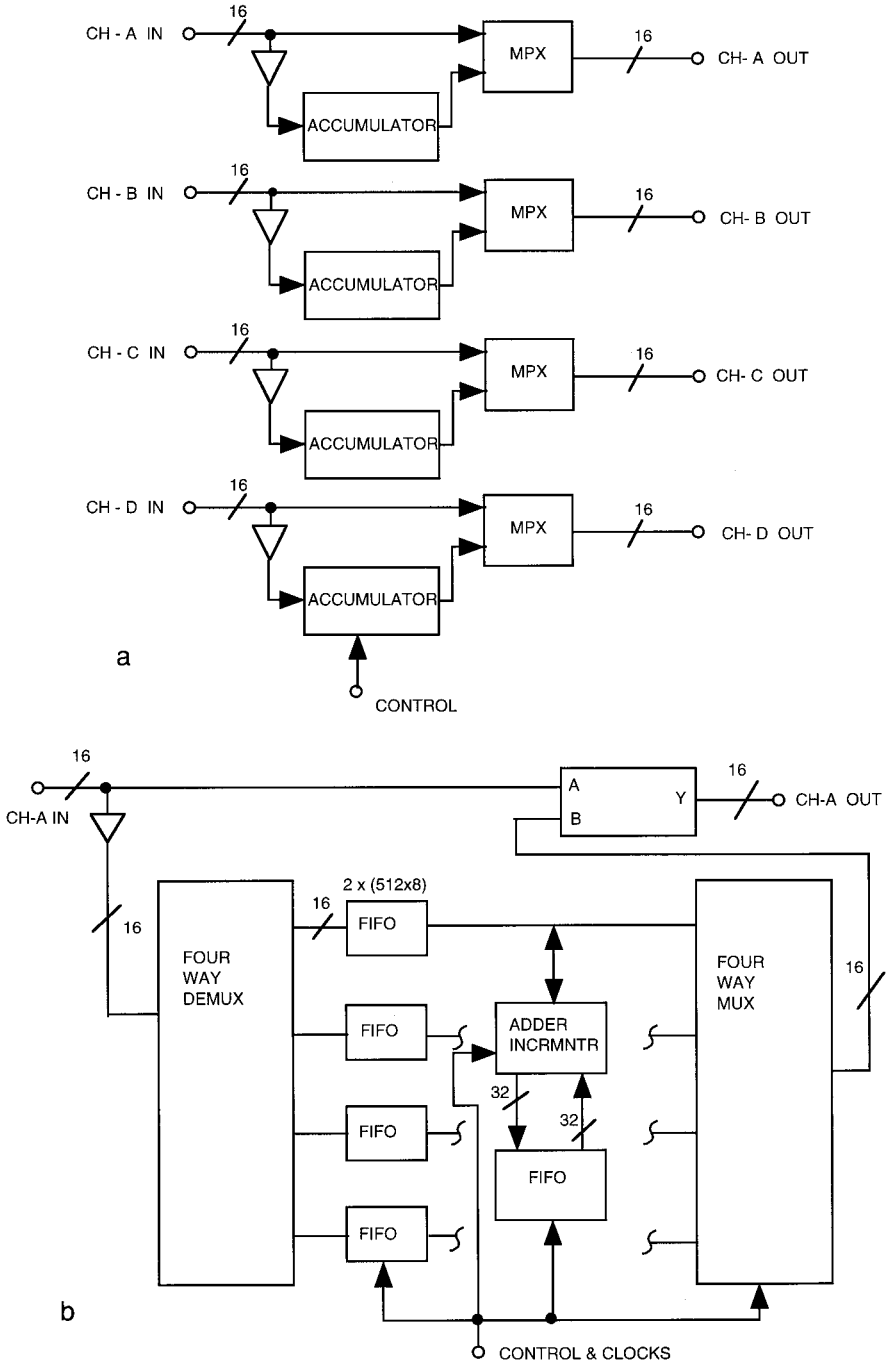

FIG. 4. Block diagram of (a) the four-channel summer and (b) the detailed data routing of one of the summer channels. (Please see text for further details.)

Magnet/gradient coil assembly. The main magnetic field was provided by a Helmholtz pair (30 cm i.d.) of water-cooled coils (GMW, Model 5451, Redwood City, CA) based on a fourth-order homogenous design. The field homogeneity was better than 10 ppm in the active volume of a cube of side 5 cm. The details of the gradient coil are reported in Ref. (*25*).

Imaging/image reconstruction. For spatial encoding of the spins, the magnetic field gradient was rotated in steps of 5° and 36 projections and 50,000 FIDs were digitized and averaged to obtain two-dimensional images. The FIDs collected were first processed with a line-narrowing exponential filter. In addition, to minimize artifacts associated with truncation, the FIDs were treated subsequently with apodization filters such as a Hamming or Kaiser filter (*29*). In our processing a Kaiser filter of order 5 was used. Finally, the FIDs were zero filled up to 64K points and Fourier transformed. Image reconstruction from

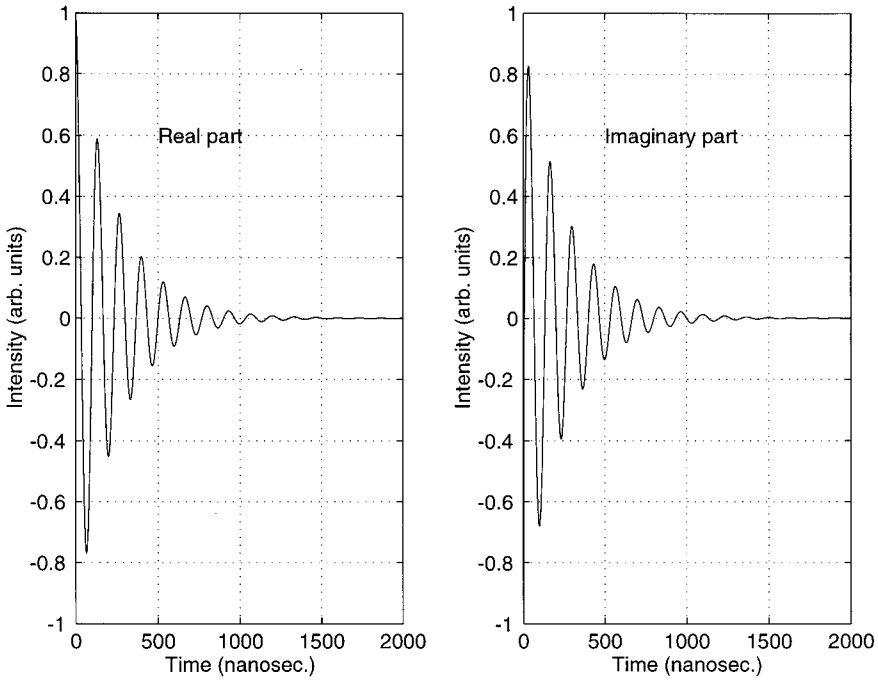

FIG. 5. Demonstration of the data acquisition system in the quadrature mode. The real and imaginary part of the FID of a sample of 1 mg of *N*-methylpyridinium tetracyanoquinodimethane (NMP-TCNQ). The origin of the *x* axis is 400 ns after the trailing edge of the RF pulse. The resonator *Q* was 25; the RF pulse width was 70 ns at a transmit power of approximately 80 W. The sampling rate was 1 GS/s, with 50,000 averages at a repetition rate of 50 kHz.

these transforms was performed using filtered-back-projection methods (*30*).

RESULTS

Quadrature-mode operation. To study the quadrature mode of operation in the EPR spectrometer, a sample of NMP-TCNQ was placed in the resonator and the FID responses were collected after excitation pulses of 70 ns width. The two quadrature components of the FID from a 1-mg sample of TCNQ are given in Fig. 5. The record length of the FIDs sampled is 4K points, at a sampling rate of 1 GS/s. The total number of FIDs averaged is 50,000 with a retrigger time of 12.5 μs corresponding to an acquisition time of 625 ms. This experiment demonstrates that a large number of FIDs can be collected and summed in a very short time and the spectra obtained upon FT show that the averaging is coherent and SNR enhancement can be achieved rapidly.

IF-mode operation. Figure 6 shows the averaging capability of the data acquisition system with the spectrometer operating in the IF mode. All other conditions such as resonators, pulse width, pulse power, and gain were maintained similar to that in the quadrature mode. The SNR improvement with number averages was evaluated and was found to follow the expected $\sqrt{2}$ law. In addition, by adapting the timing sequence shown in Fig. 2, when the signal was placed at 50.6 MHz, no significant feedthrough signal of 50 MHz was encountered.

Comparison of IF and quadrature modes. The main application of the pulsed RF EPR spectrometer developed in our laboratory is for *in vivo* imaging of small animals such as mice, infused with spin probes, having linewidths typically of about 300 mG, under a gradient of about 1 G. Such experiments require a spectral bandwidth of more than 10 MHz to be

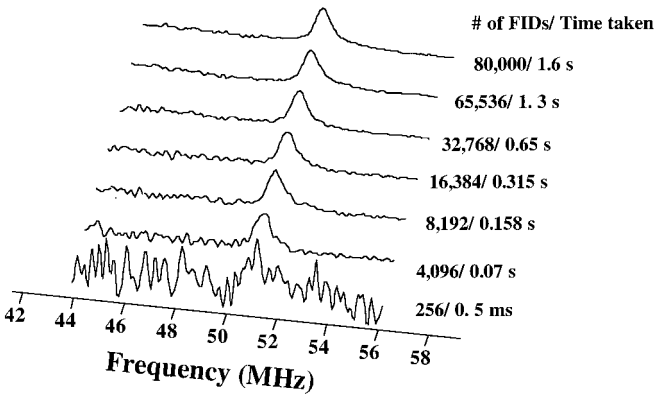

FIG. 6. Illustration of the improvement in the signal-to-noise ratio (SNR) by massive coherent averaging when the spectrometer operates in the IF mode. Phase-corrected absorption-mode spectra were obtained from the Fourier transform of coherently averaged FIDs. The spectromter parameters are identical to those given in the legend to Fig. 5, except for the number of transients coadded. These are marked in the figure, and the SNR was found to follow the expected behavior. The signals were acquired at an offset of 0.6 MHz from the carrier and no significant feedthrough at 50 MHz is seen.

sampled. Hence a comparison of the two modes of operation for variation of FID signal intensity across a bandwidth of about 11 MHz was studied. These results are presented in Fig. 7. In this figure the signal intensity under quadrature and single-channel modes are plotted against each other and the plot follows closely the excepted ratio of $\sqrt{2}$ up to an offset of ± 5 MHz.

In addition to the evaluation of the sensitivity as a function of bandwidth, an attempt was also made to compare the two modes with respect to different FID signal levels. This was achieved by varying the RF power from 3 to 80 W. At various power levels, the same number of FIDs was acquired in both the modes and averaged. The signal intensities were as expected and a plot of signal intensity as a function of square root of power was found to be almost linear (Fig. 8). The maximum flip angle was less than 90° even at the highest power (80 W) since the resonators were low-*Q* and overcoupled.

Imaging. To test the imaging capabilities of the spectrometer/imager, phantom objects placed in 50- and 80-mm-diameter resonators were studied. As was observed in prior studies, no significant loading of the resonators was observed when the resonators were loaded with an isotonic saline solution up to 90% filling factor. In a typical situation the unloaded, overcoupled resonator *Q* of 25 was reduced to around 20 when loaded up to 90% filling factor with saline solution. When phantoms were immersed in phosphate-buffered saline, the penetration of the exciting radiation was found to be minimally attenuated (*25*). The schematics of the phantoms and their placement in the respective resonators are shown in Fig. 9. Since the linewidth of the spin probe is approximately 200 mG, for resolving the phantom containing the spin probe, a gradient of 0.28 G/cm for the 50-mm-diameter resonator and a gradient of 0.21 G/cm for the 80-mm-diameter resonator were employed. These gradients correspond to a signal bandwidth of around 5 MHz. Excitation pulses of 75 and 150 ns duration were used to cover the signal bandwidth in the phantoms using the 50- and 80-mm-diameter resonators, respectively, providing spectral bandwidths of 13 and 7 MHz, respectively. The resonator *Q* was adjusted to be around 20 so as to encompass the frequency width caused by the spatial encoding of the spins in the phantom of the dimensions used with the gradients employed. The digitizing frequency (2 GHz) of the data acquisition system was more than adequate to faithfully represent the induction signals modulated by the 50-MHz IF. Two-dimensional images in the *XZ* direction were collected for both the phantoms in the corresponding resonators by using static gradients and collecting data from 36 projections. The images reconstructed by filtered-back-projection methods show that the images correspond well with the physical dimensions of the phantom.

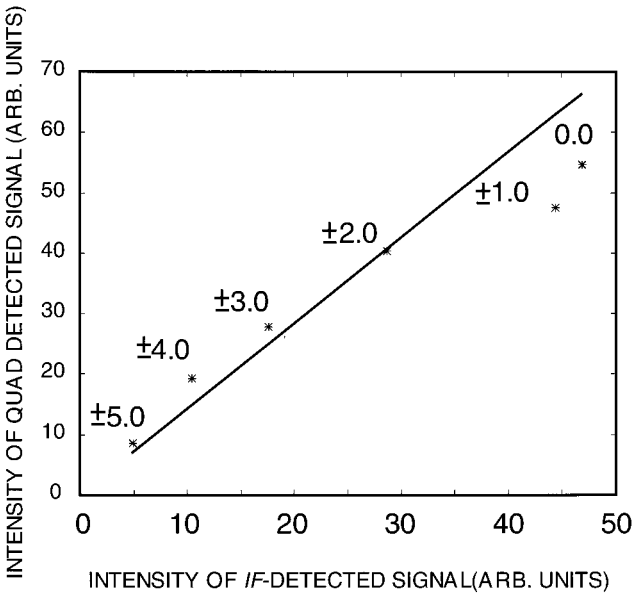

FIG. 7. Plot of the signal peak height from quadrature-mode operation against the corresponding values obtained from single-channel IF operation as a function of offset up to a range of ± 5 MHz from the carrier. The intensities were independent of the sign of the offset and are indicated in the figure in MHz. The solid line corresponds to the expected ratio of $\sqrt{2}$ between the quadrature and single-channel detection. In both cases a digital bandpass filter of 30 MHz bandwidth centered around 50 MHz was used during data processing. The pulse widths, power, number of FIDs coadded, and repetition rate were all identical (70 ns, 80 W, 50,000, and 50 kHz) in both modes.

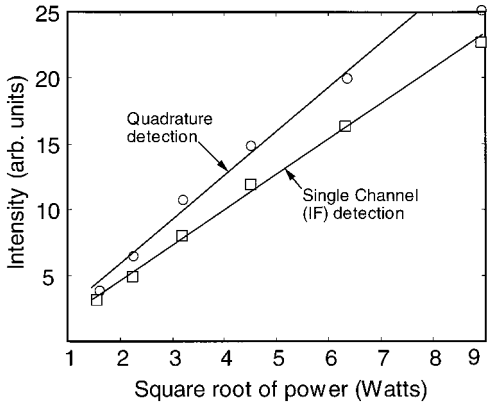

FIG. 8. Comparison of the signal intensities as a function of the square root of transmitter power at the center of the frequency range of the resonator for the quadarture mode (circles) and the single-channel IF mode (squares).

DISCUSSION

Functional information obtained by radiologic techniques in pathological conditions will provide information necessary for characterizing tissue metabolically (*1–8*). Such information, obtained by noninvasive methods, will enhance the success of therapeutic efforts. BOLD MRI, PET (*3*), ^{31}P MRS, Clark electrode oxymetry, and phosphorescence are a few techniques being evaluated to obtain functional information in a clinical setting. EPR spectroscopy can also be used to obtain functional

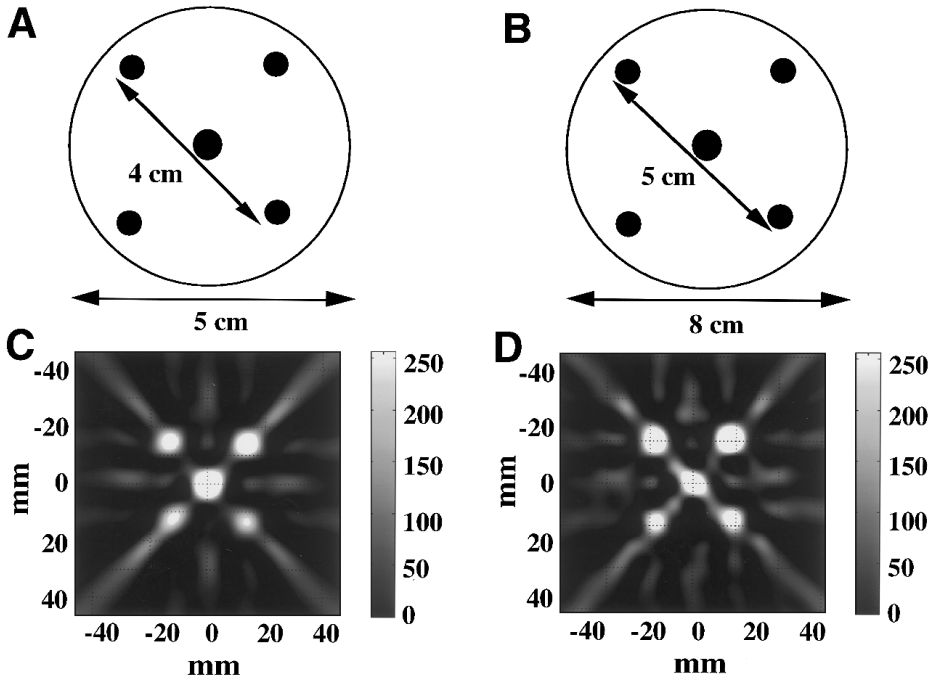

FIG. 9. 2D spatial image of a phantom containing NMP-TCNQ in five different tubes. The gradient was traversing a plane perpendicular to the tubes. (A) The five tubes were placed in the center of a 50 × 50-mm helical coil resonator occupying the corners and center of a square of side 30 mm. 100-ns pulses were used and 50,000 transients were averaged with a gradient of 0.4 G/cm and the gradient was electrically rotated through every 5° in the image plane for data collection. The imaging time was approximately 1.2 min. The resulting data were Fourier transformed and back-projected (C) using standard filtered-back-projection routines. (B) Same as in A except that the tubes were placed in an 80 × 50-mm resonator and the pulse width used for each transient was 160 ns. The five tubes occupied the corners and the center of a square of side 35 mm. In both cases the images were seen to faithfully reproduce the geometry of the phantoms with minimal distortion. It should be noted that these are not thin two-dimensional slices, but rather are projections of the spins in the tube on the transverse plane leading to the apparent diffuseness of the edge of the images.

information such as oxygen status and metabolism (*2, 6, 7*). In the presence of gradients, such information can also be spatially encoded to provide a topographical description of such vital physiological information (*2, 7*). Nontoxic exogenous spin probes are used in EPR to obtain such information, using oxygen as the endogenous contrast agent to obtain information regarding tissue oxygen status. In addition, since the half-life of the spin probes may depend on the tissue redox status, metabolic information can be obtained as well. The linewidths of most spin probes used for such studies were greater than 0.5 G and the frequency of operation in the RF, CW methods were the methods of choice, since their phase memory times were very short to permit time-domain data acquisition. CW EPR spectroscopic techniques can have limited use because of the long imaging times and also because of artifacts associated with object motion, which is in the same time scale as that needed for a single spectral acquisition. Though the time-domain methods in EPR will have comparatively minimal distortions as a result of artifact motion, such methods have not been widely used for biologic applications because of the lack of availability of appropriate spin probes with narrow linewidths as well as efficient DAS. Nontoxic water-soluble spin probes (*17, 18, 19*) possessing single narrow lines (<200 mG) permit the implementation of time-domain EPR at RF on live objects to obtain physiologic information and its development for *in vivo* application has been the focus of our attention.

Recent studies using 50 × 50-mm resonators, having a *Q* of 20, and RF pulses of 70 ns (80 W) show the feasibility of imaging spin probes in phantom objects in lossy biologic medium without any problems associated with penetration (*25*). One of the important factors making time-domain EPR a useful tool is the efficiency of the associated DAS. Several time-domain EPR spectrometers were reported (*19–22, 24*). However, some of the spectrometers (*21, 22*) utilized DAS which had fast samplers, but the repetition rates (200 Hz) did not utilize the faster dynamics of the electron spin relaxation times (<5 μs), which would, in principle, permit retrigger rates up to 0.15 MHz and enhance SNR. Efficient summation strategies that are advantageous for biologic applications of time-domain EPR to provide enhanced SNR with minimal spin probe dosage and fast image data acquisition.

Recent studies have utilized fast data acquisition systems and most time-domain EPR spectrometers are based on baseband detection (*19*) while some use detection of the FID at an intermediate frequency (*24, 25*). While both methods demonstrate the feasibility of imaging phantom objects of dimensions 5 × 5 cm, a comparative evaluation of the two receiver modes

will help in determining the optimal configuration of the receiver for individual experiments and is the focus of this study.

The quadrature mode of receiver configuration is advantageous with respect to RF power utilization (compared to conventional single-channel detection with mixing down to baseband, where only the lower half or upper half of the power spectrum is utilized); phase and image artifacts are to be addressed by CYCLOPS. In the IF mode, the same bandwidth of spectral coverage necessary for imaging experiments is afforded in a single-channel configuration. The Nyquist frequency is more than satisfied by oversampling of the IF (50 MHz), at a rate of 1 GS/s for spectroscopic experiments. However, such large oversampling might be necessary in imaging experiments, since, even at moderate field gradients, the duration of the FIDs shrinks to less than 200 ns and lower sampling rates will represent less than 200 points of information. Our sampling rate corresponds to a frequency bandwidth of 500 MHz and the frequency range corresponding to the volume of interest at the gradients we use is around 10 MHz. This will just correspond to 80 points after FT. We therefore zero fill the FIDs to 64K before FT and the spectral range corresponding to the volume of interest (VOI) is then subsampled to either 128 or 256 points before projection reconstruction to produce the images with voxel dimensions $128 \times 128 \times 128$ or $256 \times 256 \times 256$.

However, the success of the technique depends on the speed of summing individual waveforms to enhance the SNR. In the present configuration, 4K points in the FID are collected at a rate of 1 GS/s, with a 20-μs delay between successive acquisitions. The summer captures the digitized waveforms from the sampler into a 32-bit buffer. Summing and digitization processes are configured to occur simultaneously to minimize any possible delays. In the present configuration, 238,000 FIDs of 4K points can be summed in 1 s, leading to a theoretical SNR improvement of approximately 450 compared to a single FID. At this point, the speed of image data collection depends on the on-board memory available in the summer and the rate of data transfer to the host computer. A typical 2D imaging of data with the gradient rotated every 5° in the plane can be completed in less than 30 s, and the corresponding time for a 3D image with theta and phi increments of 15° intervals can be completed in 3 min. Despite using static gradients, the image data collection is efficient using time-domain data acquisition, and it is possible to collect *in vivo* pharmacokinetic images as well as spectroscopic images in almost real time. Spatial images obtained from phantom objects containing spin probes in $5 \times 5 \times 5$-cm resonators show good correspondence with the physical dimensions (*31, 32*).

Using pulses of approximately 70 ns, and RF powers up to 80 W, objects of up to $50 \times 50 \times 50$ mm were imaged in three spatial dimensions. Though a resolution of approximately 0.5 mm was obtained in the current study, it is in general determined by the linewidth of the spin probe, the gradients applied, the minimum detectable spins by the spectrometer, and the maximum spin distribution in a voxel. Preliminary experiments using water-soluble spin probes (linewidth 250 mG) suggest that a minimum of 10^{17} spins are necessary for spatial resolution of better than 1 mm using a gradients of 1 G/cm. The sensitivity and intensity will however depend on the size of the object and the magnitude of the gradients. However, when the spin distribution is absolutely uniform, at large gradients the T_2^* can become very short, requiring spin echo methods for detection.

The pulsed FT mode of operation in a single channel without the use of the quadrature mixing strategy does in fact make the spectrometer design simple and easy to implement. Preliminary results with narrow-line EPR probes on small animals and the use of endogenous oxygen as the contrasting agent show that this technique may well provide physiologically significant images and spectroscopic data that could be useful in diagnostic radiology and for guiding appropriate therapy regimens. The power of the ultrafast sampling and fast averaging that has become feasible currently does hold promise in practical applications of *in vivo* FT EPR spectroscopy and physiological *in vivo* imaging. Coupled with MRI, PET, and related imaging techniques FT EPR imaging will turn out to be an important adjunct in functional imaging. We are in the process of scaling up the resonators and further speeding up the data acquisition strategies to provide rapid imaging capabilities and obtain spatially encoded functional information.

REFERENCES

1. T. Van Gelderen, N. F. Ramsay, G. Y. Liu, J. A. Frank, D. R. Weinberger, and C. T. W. Moonen, 3-dimensional functional-magnetic-resonance-imaging of human brain on a clinical 1.5-T scanner, *Proc. Natl. Acad. Sci. USA* **92,** 6906–6910 (1995).
2. H. J. Halpern, C. Yu, M. Peric, E. Barth, D. J. Grdina, and B. A. Teicher, Oxymetry deep in tissue with low frequency electron paramagnetic resonance, *Proc. Natl. Acad. Sci. USA* **91,** 13047–13051 (1994).
3. N. F. Ramsay, B. S. Krikby, T. Van Gelderen, K. F. Berman, J. H. Duyn, J. A. Frank, V. S. Mattay, J. D. Van Horn, G. Esposito, C. T. W. Moonen, and D. R. Weinberger, Functional mapping of human sensorimeter cortex with 3D BOLD fMRI correlates highly with (H2O)-)-15 PET rCBF, *J. Cerebr. Blood F. Met.* **16**(5), 755–764 (1996).
4. M. Niiro, K. Kadota, Y. Seo, S. Nozoe, and T. Asakura, *J. Brain Sci.* **22,** 29–35 (1996).
5. H. J. Halpern, M. Peric, C. Yu, *et al.,* In vivo spin-label murine pharmacodynamics using low-frequency electron paramagnetic resonance imaging, *Biophys. J.* **71**(1), 403–409 (1996).
6. J. A. Ohara, F. Goda, K. J. Liu, G. Bacic, P. J. Hoopes, and H. M. Swartz, The pO2 in a murine tumor after irradiation—An in vivo electron paramagnetic resonance oximetry study, *Radiat. Res.* **144,** 222–229 (1995).
7. P. Kuppusamy, M. Chzhan, K. Vij, M. Shteynbuk, D. J. Lefer, E. Giannella, and J. L. Zweier, Three dimensional spectral–spatial EPR imaging of free radicals in the heart. A technique for imaging tissue metabolism and oxygenation, *Proc. Natl. Acad. Sci. USA* **91,** 3388–3392 (1994).

8. L. J. Berliner, and H. Fujii, Magnetic resonance imaging of biological specimens by electron paramagnetic resonance of nitroxide spin labels, *Science* **227,** 517–519 (1985).
9. H. J. Halpern, D. P. Spencer, J. van Polen, M. K. Bowman, A. C. Nelson, E. M. Dowey, and B. A. Teicher, *Rev. Sci. Instrum.* **60,** 1040 (1989).
10. T. Yoshimura, S. Fujii, H. Yokoyama, and H. Kamada, *Chem. Lett.* **4,** 309 (1995).
11. M. Alecci, S. D. Penna, A. Sotgiu, L. Testa, and I. Vannucci, *Rev. Sci. Instrum.* **63,** 4263 (1992).
12. P. Kuppusamy, M. Chzhan, K. Vij, M. Shteynbuk, D. J. Lefer, E. Giannella, and J. L. Zweier, *Proc. Natl. Acad. Sci. USA* **91,** 3388 (1994).
13. K. J. Liu, P. Gast, M. Moussavi, S. W. Norby, M. Wu, and H. M. Swartz, *Proc. Natl. Acad. Sci. USA* **90,** 5438 (1993).
14. P. Kuppusamy, P. Wang, and J. L. Zweier, *Magn. Reson. Med.* **34,** 99 (1995).
15. P. Kuppusamy, M. Chzhan, P. Wang, and J. L. Zweier, *J. Magn. Reson. B* **106,** 122 (1995).
16. P. Kuppusamy, M. Chzhan, P. Wang, and J. L. Zweier, *Magn. Reson. Med.* **35,** 323 (1996).
17. K. Golman, I. Leunbach, J. H. A. Larsen, G. Ehnholm, L. G. Wistrand, J. S. Petersson, and S. Vahasalo, *Acta Radiol.* **39,** 10 (1998).
18. J. H. A. Larsen, I. Laursen, I. Leunbach, G. Ehnholm, L. G. Wistrand, J. S. Petersson, and K. Golman, *J. Magn. Reson.* **133,** 1 (1998).
19. R. Murugesan, J. A. Cook, N. Devasahayam, M. Afeworki, S. Subramanian, R. G. Tschudin, J. A. Larsen, J. B. Mitchell, A. Russo, and M. C. Krishna, *In vivo* imaging of a stable paramagnetic probe by pulsed-radiofrequency electron paramagnetic resonance spectroscopy, *Magn. Reson. Med.* **38,** 409–414 (1997).
20. J. Bourg, M. C. Krishna, J. B. Mitchell, R. G. Tschudin, T. J. Pohida, W. S. Friauf, P. D. Smith, J. Metcalfe, F. Harrington, and S. Subramanian, Radiofrequency FT EPR spectroscopy and imaging, *J. Magn. Reson. B* **102,** 112–115 (1993).
21. A. Coy, N. Kaplan, and P. T. Callaghan, Three dimensional pulsed ESR imaging, *J. Magn. Reson. A* **121,** 201–205 (1996).
22. M. Alecci, J. B. Brivati, G. Placidi, and A. Sotgiu, A radiofrequency (220 MHz) Fourier transform EPR spectrometer, *J. Magn. Reson.* **130,** 272–280 (1998).
23. E. Fukushima, and S. B. W. Roeder, "Experimental Pulse NMR. A Nuts and Bolts Approach," Addison–Welsey, London (1981).
24. T. J. Pohida, H. A. Frederickson, R. G. Tshudin, J. F. Fessler, M. C. Krishna, J. Bourg, F. Harrington, and S. Subramanian, High speed digitizer/averager data-acquisition system for Fourier transform electron paramagnetic resonance spectroscopy, *Rev. Sci. Instrum.* **65,** 2500–2504 (1994).
25. R. Murugesan, M. Afeworki, J. A. Cook, N. Devasahayam, R. G. Tschudin, J. B. Mitchell, S. Subramanian, and M. C. Krishna, *Rev. Sci. Instrum.* **69,** 1869 (1998).
26. D. I. Hoult, and R. E. Richards, *Proc. R. Soc. London Ser. A.* **344,** 311 (1975).
27. C. N. Chen, and D. I. Hoult, "Biomedical Magnetic Resonance Technology," IOP, Bristol, UK (1989).
28. N. Devasahayam, R. G. Tschudin, S. Subramanian, M. Afeworki, J. A. Cook, J. B. Mitchell, A. Russo, and M. C. Krishna, Novel resonant structures for low frequency FT EPR spectroscopy and imaging, 39th Experimental NMR Conference, Asilomar, CA (1998).
29. F. J. Harris, *Proc. IEEE* **66,** 51 (1978).
30. R. K. Woods, W. B. Hyslop, R. B. Marr, and P. C. Lauterbur, *in* "EPR Imaging and in Vivo EPR" (G. R. Eaton, S. S. Eaton, and K. Ohno, Eds.), pp 91–118, CRC Press, Boca Raton, FL (1991).
31. M. Afeworki, N. Devasahayam, J. A. Cook, R. G. Tschudin, R. Murugesan, S. Subramanian, J. B. Mitchell, and M. C. Krishna, Pulsed RF FT EPR spectrometer for in vivo spectroscopy and imaging, 39th Experimental NMR Conference, Asilomar, CA (1998).
32. S. Subramanian, N. Devasahayam, J. A. Cook, M. Afeworki, T. Pohida, J. B. Mitchell, R. G. Tschudin, and M. C. Krishna, Radio frequency pulsed EPR spectroscopy and imaging. Mixing schemes to avoid quadrature detection, 39th Experimental NMR Conference, Asilomar, CA (1998).